Water Resources Research®

RESEARCH ARTICLE
10.1029/2021WR029888

Key Points:

- Bedrock groundwater (BGW) catchment area was determined from a densely measured water table in a granitic headwater basin
- BGW catchment area reflected the actual catchment effect in the bedrock layer more accurately than the surface watershed
- The boundary between two bedrock weathering classes corresponded to the hydrological basement surface; this defines the catchment area

Correspondence to:

N. Masaoka,
masaoka.naoya.7e@kyoto-u.ac.jp

Citation:

Masaoka, N., Kosugi, K., & Fujimoto, M. (2021). Bedrock groundwater catchment area unveils rainfall-runoff processes in headwater basins. *Water Resources Research*, *57*, e2021WR029888. https://doi.org/10.1029/2021WR029888

Received 3 MAR 2021
Accepted 30 AUG 2021

Bedrock Groundwater Catchment Area Unveils Rainfall-Runoff Processes in Headwater Basins

N. Masaoka[1], K. Kosugi[1], and M. Fujimoto[2]

[1]Graduate School of Agriculture, Kyoto University, Kyoto, Japan, [2]College of Science and Engineering, Ritsumeikan University, Kusatsu, Japan

Abstract Bedrock groundwater (BGW) has a contribution area that differs from that of the surface watershed. To date, there has been no analysis using BGW observations to determine to what extent the BGW catchment area influences surface runoff characteristics. This study determined the BGW catchment area from the water table, using densely nested boring wells (61 in bedrock and three in the soil layer) drilled in the granitic basin (2.3 ha). Streamflow runoff was also measured concurrently across the entire watershed (F0) and the subwatersheds (F1 to F6). The BGW catchment area of F3 accounted for 191% of the watershed area derived from surface topography, reducing the area of adjacent watersheds through cross-watershed flow. The annual precipitation input to the BGW catchment area and baseflow volume was highly correlated, indicating that the BGW catchment area reflected the actual catchment effect in the bedrock layer more accurately than the surface watershed area. The degree of bedrock weathering showed that the BGW table was distributed along the boundary of the C_L–C_M classes. The estimated actual permeability of the C_M class bedrock based on the deep percolation rate suggests that the depth near the C_L–C_M boundary is the hydrological basement surface; this defines the BGW catchment area. This study demonstrates that the BGW catchment area concept provides an accurate prediction of streamflow runoff in mountainous headwater basins that are heavily governed by hydrological processes in bedrock.

Plain Language Summary Rainfall-runoff processes in mountainous headwater basins are generally assessed in "watershed" units based on surface topography. However, bedrock groundwater (BGW) is unique in that its flow direction does not always follow surface topography and may have its own catchment area, making an accurate prediction of streamflow runoff difficult. This study determined the BGW catchment area from the contour map of the water table, using densely nested boring wells drilled in the granitic basin. The shape of the BGW catchment areas differed significantly from the surface watershed boundaries. The annual precipitation input to the BGW catchment area and baseflow volume was highly correlated, indicating that the BGW catchment area reflected the actual catchment effect in the bedrock layer more accurately than the surface watershed area. The shape of the BGW catchment area was defined by the spatial distribution of weathering degree in the bedrock layer. The boundary between two bedrock weathering classes corresponded to the nearly impermeable surface (i.e., hydrological basement surface) which controls the shape of saturated BGW table. This study demonstrates that the concept of BGW catchment area will be useful for assessing available water resources and predicting flood-related disasters in headwater basins.

1. Introduction

Surface water and bedrock groundwater (BGW) have various interactions (Sophocleous, 2002) that form unique hydrological processes in mountainous watersheds. In headwater basins (i.e., a zero-order basin), a large amount of rainwater infiltrates the soil layer and is stored as BGW in the weathered bedrock layer (K. Kosugi et al., 2006; Tromp-van Meerveld et al., 2007). Catchment storage and mean transit time of the BGW are controlled by the permeability of the bedrock (Hale & McDonnell, 2016; Pfister et al., 2017). Conversely, in foot slope areas, BGW returns to the topsoil layer, forming a constant saturation zone characterized by a unique water level variation (Haria & Shand, 2004, 2006; K. Kosugi et al., 2008; Masaoka et al., 2016). The upward flux generated by the seepage of BGW in the soil layer also triggers slope instability (Brönnimann et al., 2013). BGW plays a major role in surface runoff at the outlet of watersheds. The seepage of BGW is recognized as the main source of baseflow in streamflow discharge (Dickinson & Whiteley, 1970). Studies in weathered granitic areas have reported that this seepage accounts for more than half of the total

10.1029/2021WR029888

runoff (K. Kosugi et al., 2006, 2011). The waveform of BGW appears in the baseflow hydrograph; this waveform is often characterized by delayed peaks and gradual recession limbs in response to rainfall (K. Kosugi et al., 2011; Masaoka et al., 2016).

Notably, BGW is unique in that its flow direction does not always follow surface topography. In mountainous headwater basins, runoff rates and characteristics have been reported to differ between adjacent watersheds despite having the same geological and vegetation conditions (Inaoka et al., 2020; Komatsu & Onda, 1996; Onda et al., 2001; Uchida et al., 2005). Runoff heterogeneity is often assumed to be caused by the cross-watershed flow of BGW beyond the border on the ground surface (i.e., ridge), making assessment of water resource availability and potential for flood-related disasters difficult. Devito et al. (2005) identified risks in hydrological analysis and modeling constrained only to "watershed" units based on surface topography, and proposed that BGW may have its own contribution area. Although dense observations of BGW have been limited, Hinton et al. (1993) reported a case of high-density BGW observations within a small watershed (3.7 ha) of glacial till. They showed that the surface topography and shape of the BGW table differed significantly, and proposed that the BGW catchment area may be determined by the potential surface of the BGW table. They demonstrated that the catchment area of the small, inner small watershed differed by up to 57% between the surface topography and the BGW table. Payn et al. (2012) also assessed the spatial variability in streamflow along valleys in a mountainous watershed. They defined the subsurface contributing area as the recharge region delineated by the full collection of subsurface flow paths that discharge to a given location. This notion may be referred to as the 'BGW catchment area concept'; this concept may be the key to understanding the spatial heterogeneity of runoff in mountainous headwater basins. Although some investigations on BGW in mountains using dozens of bedrock wells have been conducted in recent years (e.g., Banks et al., 2009; Gabrielli et al., 2018; Rinderer et al., 2017), we are not aware of any analysis using field observations to determine whether a difference in the BGW catchment area creates runoff variations.

The shape of the BGW table is defined by the spatial distribution of physical properties, such as permeability, in the bedrock layer. A few studies have investigated the hydraulic properties of bedrock (Welch & Allen, 2014). Worthington et al. (2016) reported that weathering enhances the permeability of bedrock in various lithologies. In the granite region, Katsura et al. (2006, 2009) measured the hydraulic properties of the matrix in granitic rock using laboratory tests, demonstrating that this rock had sufficient permeability to allow rainfall infiltration at depths of up to several tens of meters. They also found a rough correlation between permeability and weathering degree. In contrast, many studies have reported that BGW flow is heavily influenced by preferential flow through fractures (Gleeson et al., 2009; Maréchal et al., 2004; Olofsson, 1994; Salve et al., 2012). However, the spatial distribution of fractures is heterogeneous and anisotropic; therefore, it is not possible to identify all fractures.

This study conducts detailed observations of the BGW table, where the catchment area of the BGW was determined using wells in the bedrock that were bored at a high spatial density. Alongside these observations, the relationship between runoff and the BGW catchment area was also analyzed. The relationship between the spatial distribution of physical properties and the shape of the BGW table was examined based on the distributions of the weathering degree and fractures obtained from the bedrock core sample. This study seeks to address two goals: (1) clarify the actual effect of the BGW catchment area on rainfall-runoff processes in mountainous headwater basins; and (2) identify the physical factors of bedrock that define the BGW catchment area.

2. Materials and Methods

2.1. Study Site

Observations were conducted in the Fudoji Experimental Watershed, located in the Tanakami Mountains in the southern part of Shiga Prefecture, central Japan (34°55'04"N, 135°58'54"E; Figure 1). The area is underlain by Tanakami Granite formed during the Cretaceous Period, and covered with a mixed forest consisting of *Chamaecyparis obtusa* (Japanese cypress) and several deciduous species. The mean annual precipitation in the watershed was 1,740 mm and the mean annual air temperature was 12.7°C (from 2012 to 2015).

The Fudoji Experimental Watershed is referenced by its outlet at F0 (2.3 ha), and contains six gauged subwatersheds, with outlets specified by F1 to F6 (ranging from 0.11 to 0.67 ha). Hydrological and geochemical studies were actively conducted in F3 during the early 2000s (Asano et al., 2002, 2003, 2004; Uchida et al., 2003a, 2003b, 2004). The geology and vegetation were almost uniform among the subwatersheds.

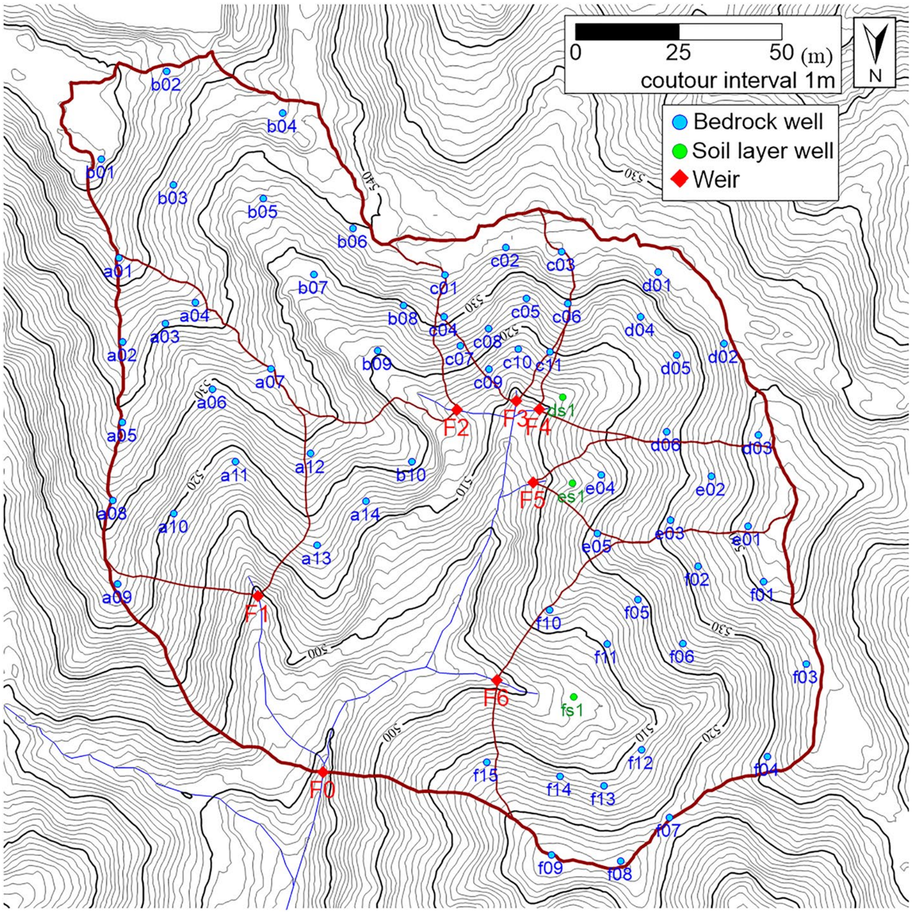

Figure 1. Topographic map of the Fudoji Experimental Watershed. Brown lines indicate surface watershed borders. Blue lines indicate the stream network.

2.2. Hydrological Observations

Streamflow runoff was measured at 5-min intervals using a V-notch weir located at the outlet of each watershed (F0 to F6; Figure 1). A rain gauge was placed ~400 m north of the F0 weir (outside of Figure 1). BGW levels were measured at 10 min intervals using a water-level gauge (OYO Corporation, S&DL mini) at 61 bedrock wells and three soil layer wells.

Evapotranspiration was not measured in this study and was estimated based on measurements at the Kiryu Experimental Watershed [KEW] (5.99 ha: 34°57'59"N, 135°59'40"E). The KEW is located ~5.5 km northeast of the study site, and has similar geology and vegetation as the F0 watershed. Thus, the evapotranspiration at KEW was considered to be approximately equal to that at the study site. Evapotranspiration at the KEW was measured from 2001 to 2008 by the eddy covariance method using fluxes measured at a height of 28.5 m on the micrometeorological observation tower. The average annual evapotranspiration was determined to be 742 mm/y, which is a near constant value regardless of the annual rainfall (Y. Kosugi et al., 2007; Kosugi & Katsuyama, 2007; Matsumoto et al., 2011).

Bedrock wells were drilled at 61 locations to depths of 3–42 m (Figure 1 and Table 1) using a hydraulic feed-type boring machine. Strainer pipes with an aperture ratio of 1.3% were installed in the unscreened portions of the wells. Casing pipes with an inner diameter of 5.1 cm were installed in the screened portion of the wells. The space between the casing pipe and the surrounding rocks was completely filled with bentonite that has a saturated conductivity near zero (<10^{-10} cm/s) to prevent preferential flow along the casing pipe. Three wells were installed in the soil layer at depths of 1–1.7 m (Figure 1 and Table 1); these wells consisted of polyvinylchloride pipes with an inner diameter of 4.4 cm, and 5-mm diameter perforations placed entirely around the periphery. These wells were manually drilled to the top of the bedrock surface.

Table 1
List of Boreholes, Including Depths of Bottom of the Well and Top of the Screening; the Shallowest, Deepest, and Average Water Levels (WL); and the Depths at the D–C_L and C_L–C_M Boundaries (Described in Section 2.3)

Name	Type	Bottom depth [m]	Depth to screening [m]	Shallowest WL [m]	Deepest WL [m]	Average WL [m]	D-C_L boundary [m]	C_L-C_M boundary [m]
a01	Bedrock	36.0	16.0	28.2	23.7	26.5	10.1	22.9
a02	Bedrock	29.0	16.0	20.5	16.6	18.9	5.9	18.4
a03	Bedrock	25.0	15.0	16.5	12.6	14.9	6.9	14.2
a04	Bedrock	28.0	15.0	20.4	17.3	19.0	9.8	11.1
a05	Bedrock	25.0	15.0	20.8	17.0	19.6	4.1	10.4
a06	Bedrock	20.0	8.4	6.4	4.2	5.2	2.2	2.2
a07	Bedrock	25.0	8.7	12.7	9.9	11.4	6.3	6.3
a08	Bedrock	25.0	13.3	17.5	14.9	16.6	6.1	7.7
a09	Bedrock	25.0	13.7	17.2	14.3	16.2	5.9	15.5
a10	Bedrock	16.0	6.2	6.8	5.1	6.1	0.7	4.2
a11	Bedrock	10.0	3.6	3.9	2.4	3.2	0.7	2.2
a12	Bedrock	25.0	11.1	13.5	11.2	12.5	4.6	9.9
a13	Bedrock	18.0	5.6	6.0	5.1	5.9	3.6	7.9
a14	Bedrock	16.0	4.0	7.0	3.9	6.4	2.4	4.0
b01	Bedrock	42.0	12.0	23.1	17.3	20.7	7.1	22.6
b02	Bedrock	29.0	13.4	15.6	11.8	14.2	14.8	20.7
b03	Bedrock	27.0	11.1	16.2	11.3	14.2	6.1	20.7
b04	Bedrock	28.0	12.1	22.7	18.9	21.2	4.9	13.9
b05	Bedrock	16.0	6.0	10.1	5.9	8.2	8.2	14.8
b06	Bedrock	20.0	9.3	16.1	11.0	14.1	7.1	12.5
b07[a]	Bedrock	7.0	0.0	4.8	1.7	4.0	-	-
b08	Bedrock	14.0	3.7	7.8	6.3	7.2	3.1	12.8
b09[a]	Bedrock	3.0	0.0	1.2	0.3	1.0	-	-
b10	Bedrock	20.0	9.2	9.6	9.4	9.5	4.6	5.6
c01	Bedrock	28.0	14.7	22.8	19.0	21.0	9.1	23.8
c02	Bedrock	27.0	15.2	20.9	15.4	19.2	9.8	24.6
c03	Bedrock	28.0	16.1	22.1	18.9	20.6	6.6	21.0
c04	Bedrock	23.0	9.4	16.3	11.4	14.0	2.9	18.5
c05	Bedrock	19.0	7.2	10.2	6.8	8.7	4.3	11.1
c06	Bedrock	19.0	8.1	14.7	12.3	13.5	5.9	12.5
c07	Bedrock	8.0	6.1	6.1	4.2	5.6	1.2	3.3
c08	Bedrock	12.0	4.2	8.5	6.0	7.2	1.4	4.7
c09	Bedrock	6.1	4.1	2.2	−0.3	1.3	0.5	0.5
c10	Bedrock	6.0	2.5	1.7	0.6	1.1	2.2	2.7
c11[b]	Bedrock	10.0	2.1	5.6	3.8	4.8	1.4	10.0

Table 1
Continued

Name	Type	Bottom depth [m]	Depth to screening [m]	Shallowest WL [m]	Deepest WL [m]	Average WL [m]	D-C_L boundary [m]	C_L-C_M boundary [m]
d01	Bedrock	28.0	15.1	18.7	15.4	17.2	6.0	14.5
d02	Bedrock	18.0	5.1	16.0	10.5	13.6	1.8	9.0
d03	Bedrock	26.0	14.2	18.7	15.0	16.8	6.2	12.0
d04	Bedrock	11.0	2.6	8.4	4.2	6.6	2.2	4.1
d05	Bedrock	13.0	2.6	8.0	3.8	6.4	1.1	12.0
d06	Bedrock	18.0	6.0	11.4	9.1	10.5	6.2	14.8
e01[b]	Bedrock	22.0	10.0	18.2	14.5	16.3	4.5	22.0
e02	Bedrock	17.0	4.9	14.7	12.1	13.5	1.0	10.8
e03	Bedrock	21.0	10.1	15.0	14.1	14.6	1.1	8.5
e04[b]	Bedrock	8.0	1.6	2.2	1.3	2.0	1.1	8.0
e05	Bedrock	21.0	10.6	15.2	13.2	14.4	2.4	9.5
f01	Bedrock	22.0	9.0	16.8	13.5	15.0	3.8	14.0
f02	Bedrock	22.0	10.2	15.3	14.5	15.0	1.0	7.0
f03	Bedrock	17.0	5.3	13.0	8.5	11.4	6.4	6.4
f04	Bedrock	18.0	6.0	9.5	7.9	8.9	2.8	8.5
f05	Bedrock	9.0	4.1	1.8	1.0	1.4	0.6	0.6
f06	Bedrock	26.0	4.1	13.2	12.3	12.7	3.5	5.3
f07	Bedrock	22.0	10.6	17.1	12.9	15.4	5.7	17.6
f08	Bedrock	25.0	12.6	21.2	17.1	19.6	7.4	9.8
f09	Bedrock	27.0	15.1	22.2	19.4	21.0	9.2	21.5
f10	Bedrock	18.0	6.0	10.5	10.0	10.2	4.9	11.9
f11	Bedrock	9.0	3.8	5.4	4.3	5.1	0.9	2.1
f12	Bedrock	10.0	3.5	6.1	3.8	4.8	2.6	4.8
f13[b]	Bedrock	10.0	5.1	9.3	6.8	8.2	2.4	10.0
f14	Bedrock	20.0	7.1	10.2	8.0	9.2	4.5	4.5
f15	Bedrock	18.0	7.1	13.7	12.3	13.1	6.9	15.5
ds1[a]	Soil layer	1.0	-	0.8	0.2	0.7	-	-
es1[a]	Soil layer	1.0	-	0.8	0.0	0.7	-	-
fs1[a]	Soil layer	1.7	-	0.9	0.1	0.5	-	-

Note. All values indicate depths in meters from the ground surface.
[a]No core sample obtained at b07, b09, and soil layer wells. [b]Not reach the depth of C_M class.

2.3. Physical Properties of Boring Core

Boring core samples were collected from all bedrock wells, with the exception of b07 and b09. Granite cores are generally classified into four categories based on weathering degree, color, and hardness of the rock: *A*, *B*, *C*, and *D* (Table 2; Japanese Geotechnical Society, 1979). Class *A* represents unweathered granite, and the class letter advances in the Latin alphabet with the degree of weathering. Classes *C* and *D* are divided again into three subordinate categories, that have the subscripts *H*, *M*, and *L* designating high, medium, and low hardness, respectively. The cores obtained in this study were classified as classes *D* (with no distinction between D_L, D_M, and D_H), C_L, C_M, C_H, and *B*. The depths of the D–C_L and C_L–C_M boundaries are summarized in Table 1. For wells that did not reach the C_M layer (i.e., c11, e01, and e04), the bottom of these wells was considered the C_L–C_M boundary.

Table 2
Weathering Classification of Granite Rock (Japanese Geotechnical Society, 1979; Katsura et al., 2009)

Weathering class	Degree of weathering	Color	Hardness
D_L	Entirely weathered Most of feldspar is generally altered into clay Quartz is decomposed into fine grains	Yellowish brown	Very soft Powdered by finger pressure
D_M	Entirely weathered Most of feldspar is generally altered	Yellowish brown	Very soft Crushed by finger pressure
D_H	Entirely weathered Plagioclase is altered into clay	Yellowish brown	Soft Crushed by finger pressure
C_L	Weathered entirely while retaining rock fabric and structure Plagioclase is generally altered Quartz is left unweathered	Light yellowish brown to yellowish brown	Soft Partly crushed by finger pressure
C_M	Weathered except inside rock body Plagioclase and biotite are altered further	Grayish brown to light yellowish brown	Slightly soft to hard Easily split when hammered
C_H	Weathered along fractures Plagioclase and biotite are partly altered	Brownish gray to (light) grayish brown	Moderately hard Emits a dull clank when hammered
B	Generally fresh	Milk-whitish gray to (light) brownish gray	Hard Emits a light clank when hammered
A	Fresh	Bluish gray to milk-whitish gray	Very hard Emits a clank when hammered

Data on the rock fracture and the rock quality designation (RQD; Deere, 1968) was measured from the cores. The RQD is an index indicative of the rock mass, and is expressed as the ratio of the total length of cores that have a length exceeding 10 cm per unit interval (1 m). Figure 2 shows the frequency distribution of the RQD for each weathering class in all boreholes utilized in this study; the RQD was not measured for class D. The RQD tended to decrease with advanced weathering; however, the RQD distributions were similar between classes C_M and C_L, suggesting that the fracture density was comparable in these classes.

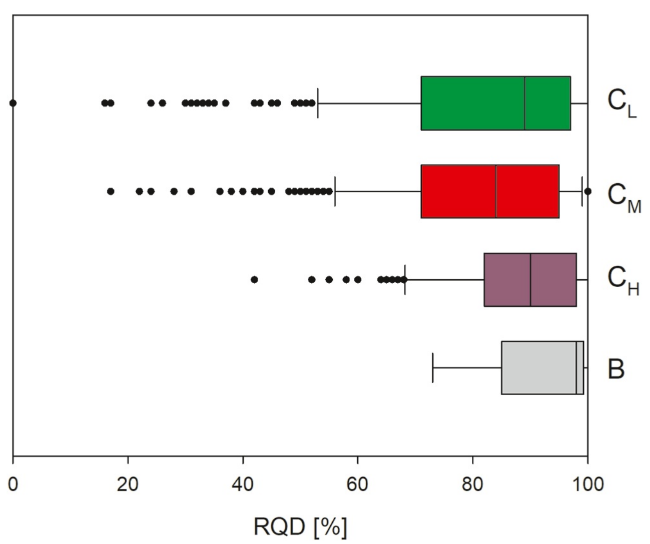

Figure 2. Frequency distribution of the rock quality designation for each weathering class in all boreholes used in this study. Box and whisker plots denote the median, 10th, 25th, 75th, and 90th percentiles. Dots denote outliers.

2.4. Baseflow Separation

Baseflow is a streamflow component that responds slowly to rainfall, and is usually associated with water discharged from the stored BGW. To separate the streamflow into response flow and baseflow, a widely used hydrograph separation method was applied (Hewlett & Hibbert, 1967). The method uses a line with a constant slope to interpolate the baseflow hydrograph during a storm event. The line connects the last point before the rise, with the point at which it intersects the recession curve. To determine the end point of the line, the hydrograph was plotted semi-logarithmically, and a polygonal line was fitted to the recession curve. The second folding point of the polygonal line is identified as the point in time at which the response flow ceases, and the streamflow is entirely made up of baseflow (Jitousono & Haruyama, 1985). We reviewed event hydrographs for the F0 watershed (F0) with total precipitation exceeding 20 mm. Then an optimal slope value of 0.01 mm/h/d was empirically determined so that the end point of the line coincided with the cessation point of the response flow. This optimal value was then applied uniformly to the hydrographs of the other subwatersheds (F1–F6) to automatically calculate the baseflow.

2.5. Bedrock Groundwater Catchment Area

The contour maps of the BGW table were illustrated for three time periods: the dry period, the wet period, and the annual average. Instances when baseflow was at a minimum or a maximum for the F0 watershed were defined as dry and wet periods, respectively. On the assumption that the ground surface and the BGW table coincide in the river channel experiencing perennial streamflow, the auxiliary BGW level was used to draw the contour maps.

When vertically infiltrated rainwater reaches the saturated BGW table, it flows in the steepest gradient direction (orthogonal to the contour) as saturated lateral flow. As such, a unique catchment area may be determined on the BGW table (Hinton et al., 1993). However, in the downstream region of the watershed (near the weir), the BGW is considered to spring out onto the bedrock surface and flow along the ground surface topography. For this reason, a unique method was used to define the BGW catchment area. In the upstream and middle regions of the watershed, the BGW catchment area is bounded by the ridgeline of the BGW table extracted using the Quantum Geographic Information System 3.4 flow direction function (Garbrecht & Martz, 1997). On the downstream side from where the BGW ridgeline intersects the surface watershed border, the BGW catchment area coincides with the surface watershed border. For the area in contact with the outer edge of the F0 watershed, the BGW catchment area coincides with the edge.

2.6. Runoff Ratio

In general, the relationship between the area, runoff, and precipitation may be expressed by Equation 1, assuming that there is no change in water storage before and after the period being investigated (Dooge, 1957):

$$\mathrm{QV} = c \times \mathrm{PV} \tag{1}$$

where QV, c, and PV are the volumetric runoff (m^3/y), runoff ratio, and volumetric precipitation (m^3/y), respectively. In this study, the QV of the total runoff and baseflow (QV_T and QV_B, respectively; m^3/y) were compared with the PV input to the surface and BGW catchment area ($\mathrm{PV}_{\mathrm{SF}}$ and $\mathrm{PV}_{\mathrm{BG}}$, respectively; m^3/y) for each watershed/subwatershed.

3. Results

3.1. Runoff

The total runoff and baseflow hydrographs for one water year from October 1, 2014, to September 30, 2015, are shown in Figure 3b (we call 2015 water year hereafter). Instances when baseflow was at a minimum or a maximum for the F0 watershed were defined as dry and wet periods, respectively (denoted by the broken lines in Figure 3). The F0 area-normalized hydrograph may be considered the average waveform of runoff from the subwatersheds. Among the subwatersheds (F1 to F6), the F1, F2, and F6 area-normalized hydrographs exhibited similar runoff waveforms to that in F0. The F3, F4, and F5 area-normalized hydrographs had runoff waveforms in which the amplitude of runoff response was smaller than that in F0. In F3, the fluctuation in baseflow was particularly low and stable.

Figure 4 presents the annual precipitation, total area-normalized runoff (Q), and area-normalized baseflow (Q_B). Annual precipitation was 1863.5 mm (100%). The Q ratio in the F0 watershed was 47.8%; the F1, F5, and F6 watersheds also had similar Qratios. The Q ratio in F3 was by far the highest in all watersheds, reaching 75.6%. Conversely, the Q ratios were low in F2 and F4, which were adjacent to F3, at 19.7% and 21.0%, respectively. Differences among the Q_B ratios were also substantial, which appeared to constitute the bulk of the variation in the Q ratio. The baseflow index (Q_B/Q) was 70.7% in F0, and the average value in all watersheds was 76.9%; this demonstrates that the baseflow significantly contributes to discharge in all the watersheds.

The evapotranspiration is shown in Figure 4 as a reference. The F3 subwatershed demonstrated a noticeable imbalance of the water budget based on ET estimates from the KEW.

3.2. Shape of Bedrock Groundwater Table

Figure 5 presents the contour maps of the BGW table for the three time periods. The timings of the dry and wet periods are provided in Figure 3. The BGW table roughly corresponded to the ground surface topog-

10.1029/2021WR029888

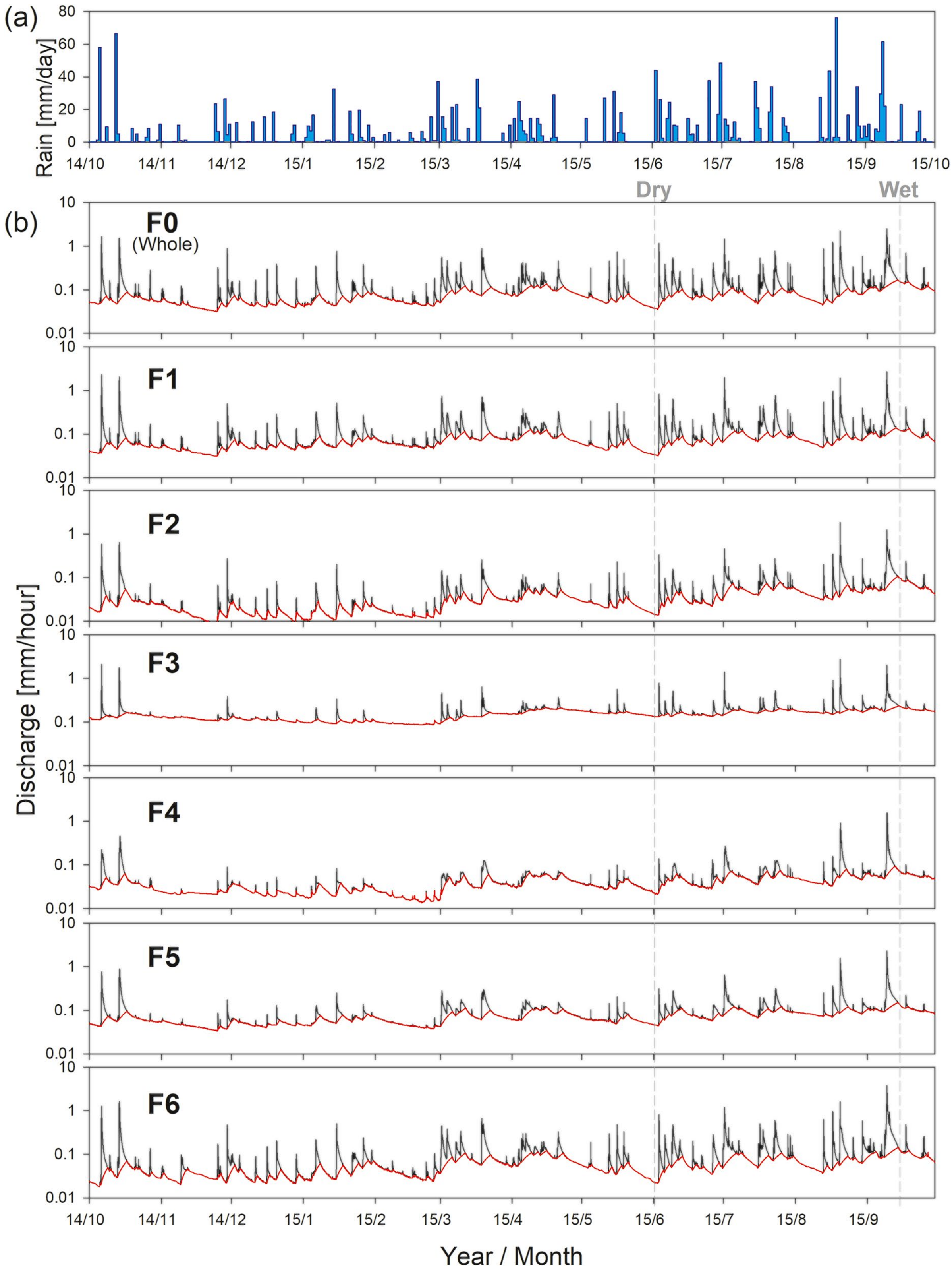

Figure 3. (a) Hyetograph; and (b) discharge hydrographs in watershed F0 to F6 for 2015 water year. Black and red lines indicate total runoff and baseflow, respectively.

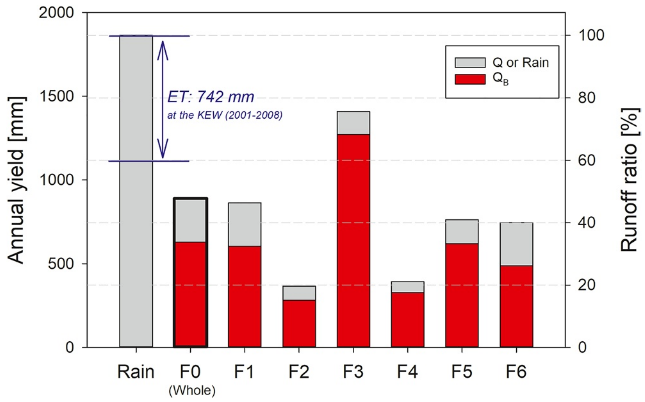

Figure 4. Annual yields of rainfall, total runoff (Q), and baseflow (Q_B) shown in units of height in mm and ratio as a percentage in the 2015 water year. The annual average evapotranspiration measured at the Kiryu Experimental Watershed is also shown.

raphy (Figure 1), although it contained gentler undulations. In general, the BGW in the F0 watershed was gathered from either side of the central valley line (the valley from F3 to F0). The ridges of the BGW table corresponding to the border of the subwatersheds (e.g., F1 and F2) were unclear. The topography of the BGW table had less relief than that of the ground surface, particularly for the F3 watershed.

Focusing on the differences between periods, the BGW level increased by up to 5 m in the upstream region of each watershed during the wet period (Figure 5b), compared to the dry period (Figure 5a). However, no significant change in the BGW level occurred in the downstream region and the BGW divides were relatively constant. The annual average of the BGW table (Figure 5c) was similar to that of the dry period (Figure 5a), suggesting that higher BGW levels were transient.

3.3. Bedrock Groundwater Catchment Area

The shape of the BGW catchment areas for the subwatersheds shown in Figure 5 differed significantly from the subwatershed boundaries suggested by surface topography. Although there were slight differences depending on the period (a to c), the shape of the BGW catchment area was roughly the same. The area between F1 and F2 does not belong to either of these watersheds, and is considered to belong to the F0 BGW catchment area; the same applies to the area between F5 and F6. The area located upstream of F2 does not belong to the F0 watershed, indicating that the BGW flows out of the watershed. Notably, the F3 BGW catchment area expanded to the left and right from the surface watershed border, reducing the BGW catchment areas of F2 and F4. The high runoff ratio in F3 and low runoff ratio in F2 and F4 (Figure 4) corresponds to higher and lower BGW catchment areas, respectively, than those drawn from surface topography.

As the BGW catchment area (Figure 6) did not change significantly (based on apparent wetness conditions), the discussions herein focus on the annual average (Figure 5c). The BGW catchment area of F3 was 191% of the watershed area derived from the surface topography. These values were approximately the same in the F5 subwatershed. In other subwatersheds, the BGW catchment area was smaller than the surface watershed area, especially in the F2 and F4 subwatersheds, where the ratios were 47% and 62%, respectively.

3.4. Runoff Ratio

We compared the relationships between PV_{SF} and QV_T for watersheds F0 to F6 (Figure 7a). While PV_{SF} explained much of the variation in QV_T, subwatersheds F2, F3, and F4 fell well off a line that would indicate a constant runoff ratio. The relationship between PV_{SF} and QV_B showed the same tendency (Figure 7b). In the relationship between PV_{BG} and QV_T and QV_B (Figures 7c and 7d, respectively), there was very high linearity, with little variation from a constant runoff ratio.

Figure 7 also presents the straight line in which Equation 1 is fitted to each plot using the least squares method, and the coefficient of determination r^2 for each fitting. The r^2 values of QV_T and QV_B for PV_{SF} were 0.87 and 0.84, respectively, and those for PV_{BG} were 0.98, and 0.99, respectively.

3.5. Bedrock Groundwater Versus Weathering Degree

Figures 8b and 8c illustrate the boundary surfaces of the bedrock weathering classes D–C_L and C_L–C_M (Table 2), respectively. The topography of the D–C_L boundary (Figure 8b) roughly corresponds to ground surface topography (Figure 8a). At the surface watershed border on the left and right of the F3 watershed (denoted by brown lines), the topography of the D–C_L boundary is ridge-shaped. In contrast, the topography of the C_L–C_M boundary (Figure 8c) is highly depressed in the middle to upstream region of F3 (i.e., wells c01 to c06). As a result, the ridge line on the left side bends toward F2, while the ridge line on the right side bends toward F4. The ridge lines of the C_L–C_M boundary did not correspond to the surface watershed bor-

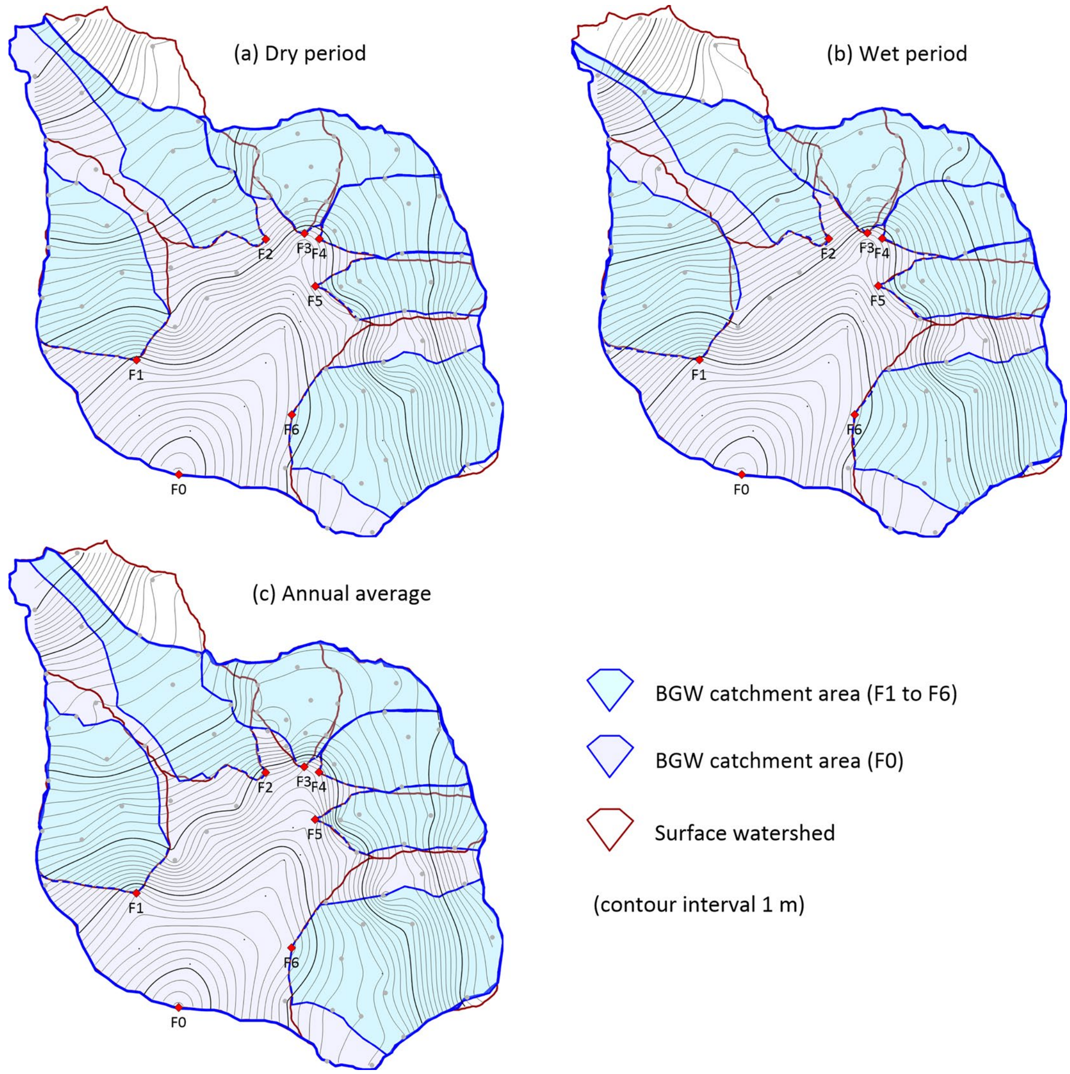

Figure 5. Contour maps of bedrock groundwater (BGW) table during (a) the dry period; (b) wet period; and for (c) the annual average. Gray circles denote boreholes, and dots denote dummy points used for drawing the BGW contour map. Border lines of the surface watershed and the BGW catchment area are also shown. The BGW catchment area is bounded by the ridgeline of the BGW table in the upstream and middle regions (denoted by blue lines) and coincides with the surface watershed border in the downstream region (denoted by the blue broken lines).

der; however, it roughly corresponds to the BGW catchment area border (denoted by blue lines). The BGW table (Figure 8d) shows a very flat surface in the region (i.e., wells c01 to c06), in the same location as a large depression of the C_L–C_M boundary.

Cross-sectional profiles of the weathering classes allow detailed examination of the BGW behavior around F3 (Figures 8 and 9). The first cross-section (Figure 9a) passes through the valley line at the center of F3. The bedrocks of the D and C_L classes were thickly distributed at wells c02 and c05, in the upstream part of the slope. A close observation of the core of well c02 shows that the C_L bedrock occurs at a BGW level of 511–513 m under the C_M and C_H bedrock. As a result of such discontinuous weathering, the C_L–C_M boundary was extremely flat between wells c02 and c10. The BGW table was located immediately above this boundary, showing a similarly flat shape. The second cross-section (Figure 9b) passes through the ridge top between watersheds F2 and F3. At wells c01 and c04 in the upstream region, the C_L bedrock was present in the deep part at a BGW level of ~513–515 m, as well c02. However, the D and C_L bedrock was thin at well c07. As a result, the C_L–C_M boundary was raised from wells c04 to c07, contrary to the slope. The BGW table

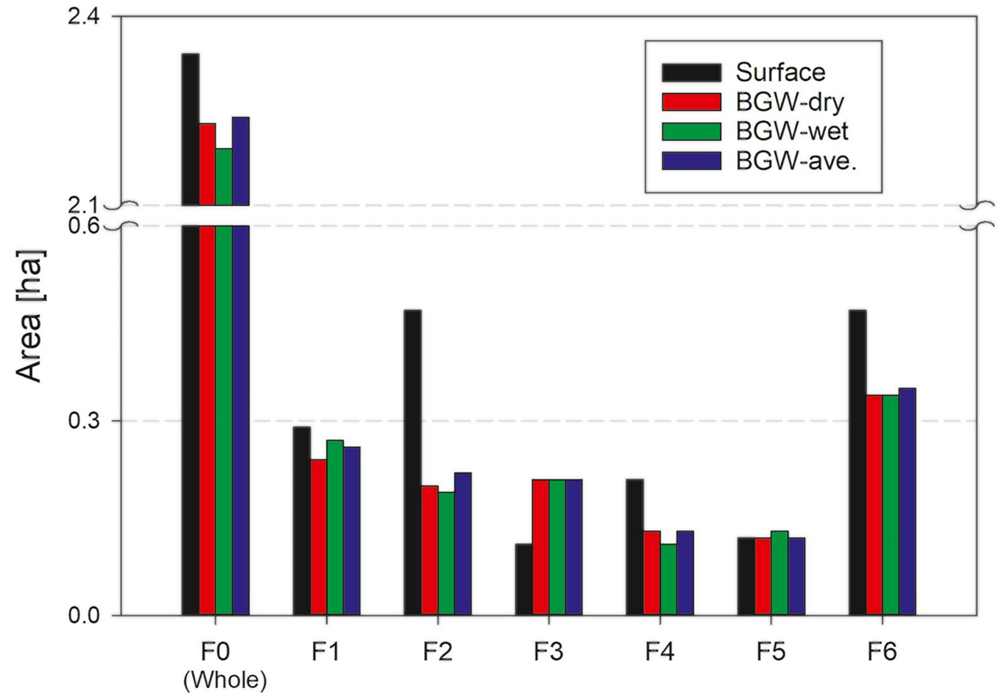

Figure 6. Surface watershed areas, and the bedrock groundwater catchment areas during the dry and wet periods, and the annual average.

is distributed along the C_L–C_M boundary, exhibiting a reverse slope. This indicates that the BGW in well c04 does not flow into c07. The third cross-section (Figure 9c) crosses the midstream of F3, perpendicular to the valley line. Unlike the ground surface topography, the C_L–C_M boundary is characterized by a wide valley shape at wells c04, c05, and c06. The BGW table is distributed along the C_L–C_M boundary and shows cross-watershed flow from F2 (b08) and F4 (d04) to F3. The BGW at well c04 was observed to flow into c05 on the side (Figure 9c) (as opposed to the c07 well downstream (Figure 9b), and then flows to the F3 weir (Figure 9a).

4. Discussion

4.1. Bedrock Groundwater Catchment Area Versus Runoff Ratio

The catchment area determined by the shape of the observed BGW table rather than the surface topography accurately reflected the actual contribution area to the baseflow volume. QV_T was not highly correlated with PV_{SF} (Figure 7a). Among the runoff components, there was a large variation in the response flow which is likely to fluctuate because of the distribution of the saturated zone in the watershed (e.g., Waddington et al., 1993). However, QV_B, excluding the response flow, did not have a high correlation with PV_{SF} (Figure 7b). As the geology, topography, or vegetation are similar among the subwatersheds, this variation is most likely attributable to cross-watershed BGW flow due to the bedrock structure.

Previous studies in the granitic area have shown that most baseflow is formed by BGW seepage (K. Kosugi et al., 2006, 2011), which implies a close relationship between baseflow volume and the BGW catchment area. The very high r^2 value of PV_{BG} for QV_B (0.99; Figure 7d) suggests that the baseflow runoff ratio calculated using the BGW catchment area was nearly uniform across all subwatersheds. This indicates that the BGW catchment area, determined by the shape of the observed BGW table, accurately reflects the actual contribution of the bedrock layer to the watershed outlet. The runoff ratio generally varies because of the subsurface bedrock structure that characterizes mountainous headwater basins (e.g., Uchida et al., 2005).

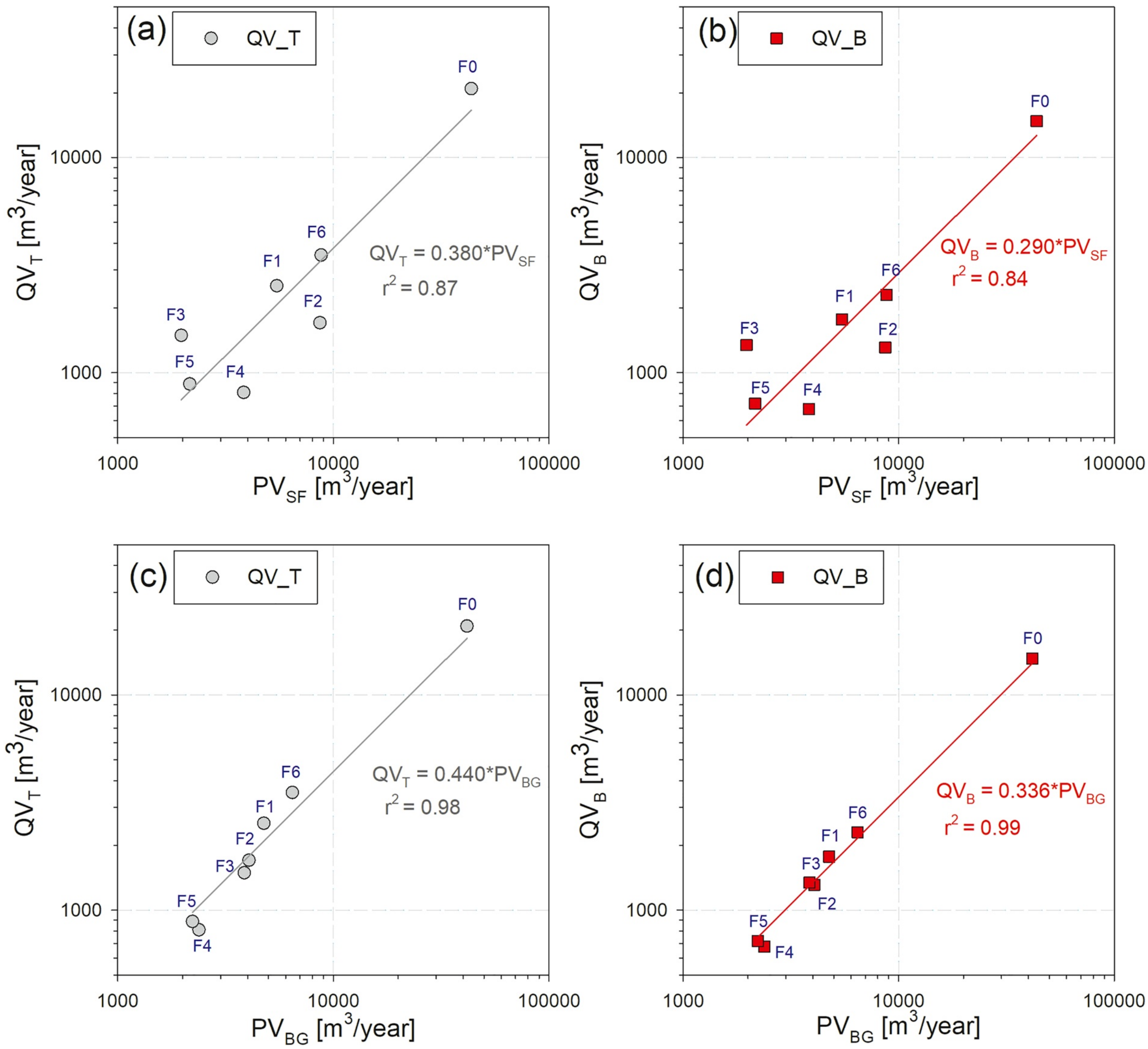

Figure 7. Scatter plots showing (a) volumetric precipitation input to the surface watershed area (PV_{SF}) versus volumetric total runoff (QV_T); (b) PV_{SF} versus volumetric baseflow (QV_B); (c) volumetric precipitation input to the bedrock groundwater catchment area (PV_{BG}) versus QV_T; and (d) PV_{BG} versus QV_B in 2015 water year. Fitted lines of Equation 1 and determination coefficient (r^2) are also shown. Watershed numbers are denoted by characters located next to points.

However, the variation in the area-normalized discharge may be eliminated and proper hydrograph interpretation is enabled by recognizing that the BGW divides differ from the surface divides (i.e., Figure 5).

4.2. Water Budget

The runoff ratio and deep percolation rate in the study watershed were accurately estimated by considering the BGW catchment area. The c of the QV_B based on the BGW catchment area was 0.336 (Figure 7d). The average percentage of precipitation partitioned to baseflow was 33.6% in the watershed investigated in this study, with a BGW catchment area of 0.13–2.24 ha. This is consistent with the results of previous studies on a granitic basin. In the KEW, it was estimated that 28.2%–30.8% of the annual precipitation in the 0.086 ha watershed was baseflow, which was seepage water from bedrock (K. Kosugi et al., 2006). In another 2.1 ha granitic basin (the Nishi'otafuku-Yama Experimental Watershed, Japan), the baseflow as bedrock seepage was estimated to be 33.9% of the annual precipitation (K. Kosugi et al., 2011).

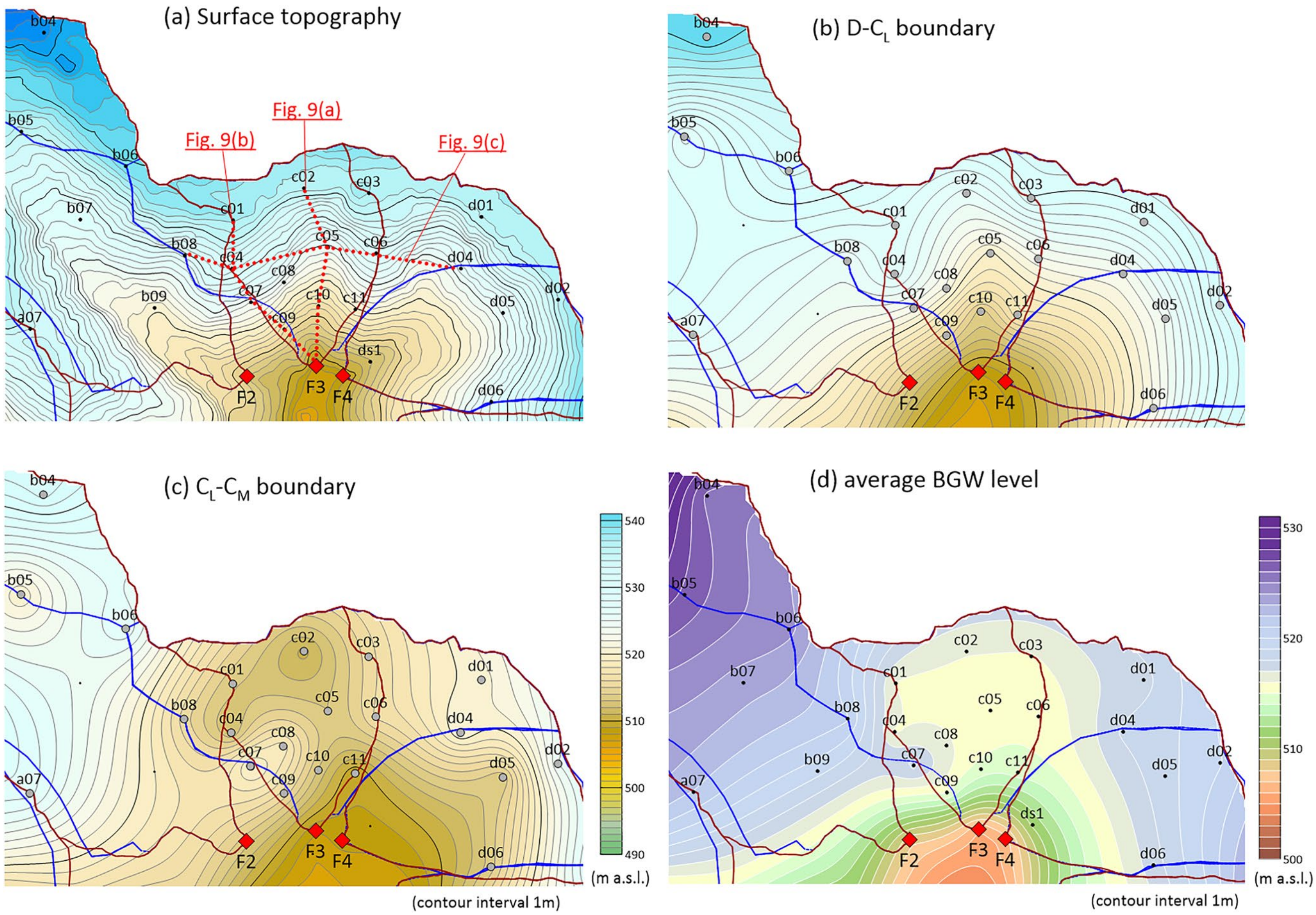

Figure 8. Topographic maps of (a) ground surface; (b) weathering surface at D–C_L boundary; (c) C_L–C_M boundary; and (d) map of the annual average bedrock groundwater (BGW) table around the F3 watershed. Brown and blue lines denote the border lines of the surface watershed and BGW catchment area, respectively.

QV_T was highly correlated with PV_{BG} ($r^2 = 0.98$; Figure 7c). As the baseflow index (Q_B/Q) was high at 76.9% on average (Figure 4), and the runoff ratio of QV_B was nearly uniform as a result of the BGW catchment area (Figure 7d), the runoff ratio of QV_T also approached uniformity across all subwatersheds. The c of QV_T based on the BGW catchment area was 0.440 (Figure 7c), indicating that the average percentage of precipitation partitioned to total runoff for the F0 watershed was 44.0% and water loss was 56.0%. In this study, water loss consists only of evapotranspiration and deep percolation, and is assumed to exclude cross-watershed BGW flow as the BGW divides are considered. Based on the evapotranspiration (742 mm/y, 39.8% of annual precipitation; Figure 4), the deep percolation rate was estimated to be 16.2% (301.9 mm/y), which was slightly higher than that in the KEW (0%–10%; Matsumoto et al., 2011).

4.3. Bedrock Groundwater Versus Weathering Degree

The boundary of the weathering class is likely to correspond to the impermeable surface in the bedrock. Despite fluctuations in the BGW level due to rainfall infiltration, the shapes and catchment areas of the BGW contributing areas showed little seasonal change (Figures 5 and 6). This indicates that the BGW catchment area is defined by the physical properties of the bedrock, with little change over time. The distribution and flow of BGW around the F3 watershed corresponded to the weathering surface (i.e., the C_L–C_M boundary) in the bedrock layer, as opposed to the ground surface topography (Figure 8). The BGW table is distributed along the C_L–C_M boundary and shows cross-watershed flow from F2 and F4 to F3 (Figure 9). These results

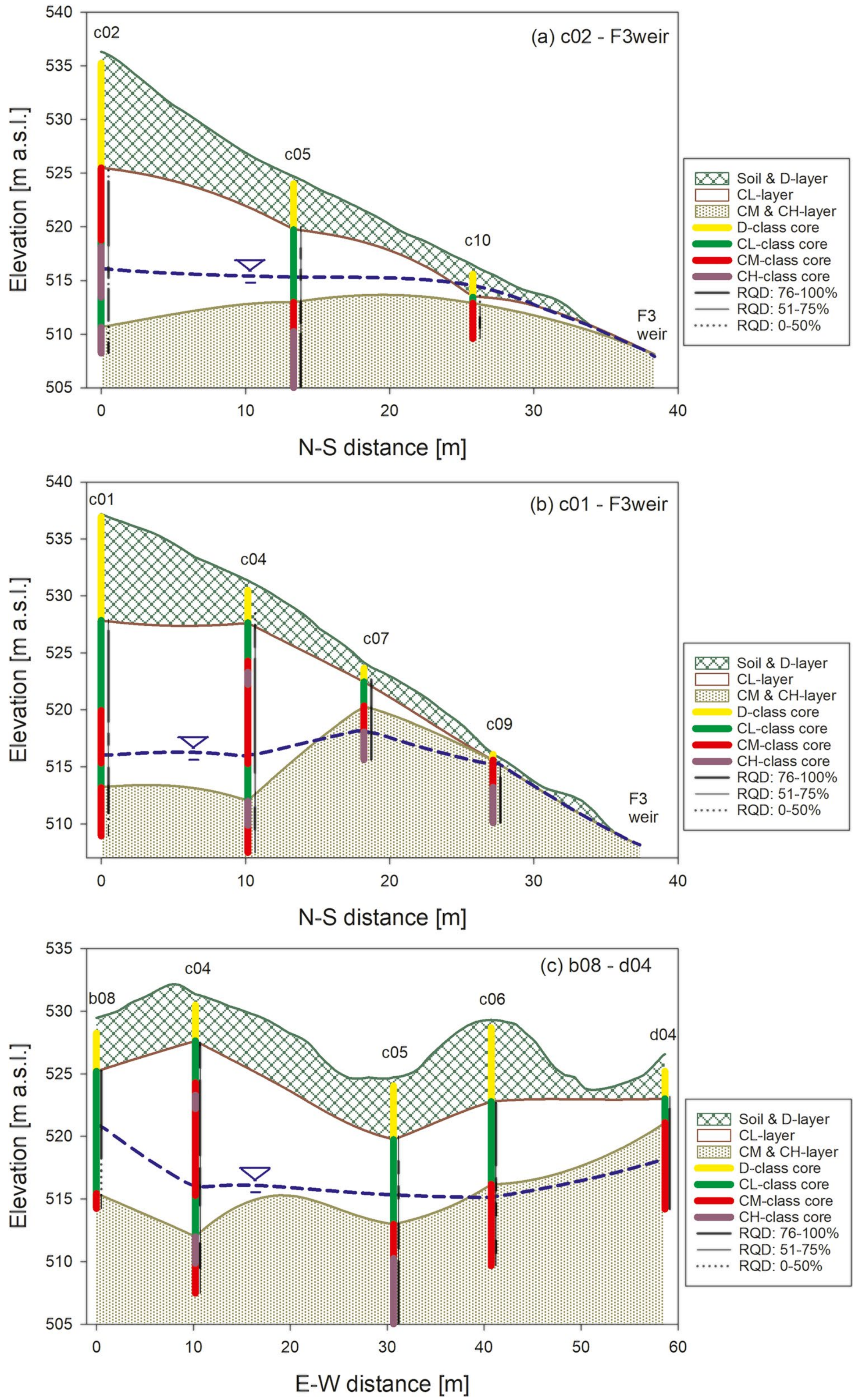

Figure 9. Vertical cross-sectional maps showing the weathering class and the rock quality designation of bedrock. The locations of cross-sections (a–c) are shown in Figure 8a. Broken blue lines denote the bedrock groundwater table (annual average).

Table 3
The Core-Scale Matrix Saturated Hydraulic Conductivity (K_s) of Granitic Bedrock (Katsura et al., 2009)

	Matrix saturated hydraulic conductivity (Ks)		
Weathering class	[cm/sec]	[mm/hour]	[mm/year]
Soil	0.069	2500	2.2E+07
D_L	-	-	-
D_M	2.2E-05	0.79	6,900
D_H	1.3E-04	4.7	4.1E+04
C_L	1.7E-05	0.61	5,400
C_M	8.3E-09	3.0E-04	2.6
C_H	-	-	-

suggest that the C_L–C_M boundary is an impermeable surface in the bedrock, which means a hydrological basement surface.

4.4. Hydrological Basement Surface

The saturated hydraulic conductivity (K_s) of the bedrock cores and the deep percolation rate also suggest that the C_L–C_M boundary corresponds to the hydrological basement surface. Katsura et al. (2009) conducted physical tests on soil and bedrock core samples obtained from two granitic areas in Japan, and measured the K_s values (Table 3). When the units were converted to hourly values, the K_s of soil was 2500 mm/h, which is much larger than the maximum hourly rainfall recorded in Japan (187 mm/h; Imamoto et al., 1984). In contrast, the K_s of the D and C_L class bedrock was 0.61–4.7 mm/h, indicating that most rainfall cannot infiltrate when its waveform is directly input. However, when the units were converted to a yearly value, the K_s result in 5,400 mm/y, even in the C_L layer; this is higher than the annual rainfall of 1863.5 mm/y in the 2015 water year at the study site. If rainfall intensity is moderated by the buffer effect of the thick soil layer, a large amount of rainfall can evidently infiltrate into the D and C_L layers (K. Kosugi et al., 2006). Regardless, the K_s of the C_M class bedrock is 2.6 mm/y, which means that rainfall is barely able to infiltrate into this layer despite the extent to which rainfall intensity is moderated by the thick soil layer and the D and C_L class bedrock layers.

As the actual K_s of the C_M layer includes the influence of fractures, it is considered higher than the matrix K_s to some extent. Section 4.2 states that the estimated deep percolation was 301.9 mm/y (9.6E-7 cm/sec) in the F0 watershed. This value is an intermediate value between the matrix K_s of the C_L and C_M layers (Table 3), implying that the actual K_s of the C_M layer approximates to this value. As described above, it was inferred that the depth near the C_L–C_M boundary is an almost impermeable surface in the bedrock; the hydrological basement surface.

The BGW catchment area is defined by the shape of the hydrological basement surface. Additionally, the depth of the hydrological basement surface provides highly useful information to assess the available water resources and model water level fluctuations. The results of this study indicate that the depth of the hydrological basement surface may be determined based on the degree of bedrock weathering, which can be associated with the general classification of the bedrock permeability by Welch and Allen (2014). They referred to the D and C_L layers as "saprolite-highly weathered bedrock layer" having the K_s of 1.0E-5 to 1.0E-3 cm/sec. The deepest layer observed was referred to as "low-K bedrock layer" having the K_s of 1.0E-7 to 1.0E-4 cm/sec, corresponding to the actual K_s of the C_M layer estimated from the deep percolation rate (9.6E-7 cm/sec). Our results indicate that the surface of "low-K bedrock layer" (Welch & Allen., 2014) can be regarded as the hydrological basement surface which controls the shape of saturated BGW table and base flow volume.

Based on the distribution of the vertical weathering degree in the cores (Figure 9), there were multiple boundaries where the weathering degree exceeded the C_M at the c01, c02, and c04 wells. However, a deeper boundary corresponded to the water table. Near these wells, water flows obliquely downward through the surrounding strongly weathered sections as opposed to the vertical infiltration through unweathered sections. Thus, a deeper C_L–C_M boundary matched the hydrological basement surface.

4.5. Fracture Distribution

Highly fractured regions of well cores tended to be isolated and separated by less fractured materials, suggesting that fractures are more likely to contribute to lateral water movement than vertical percolation. Figure 9 also shows the vertical distribution of the RQD, which reflects the fracture density. The RQD was irregularly distributed in the vertical direction in all wells. It is possible that the highly fractured bands (i.e., RQD $<$ 75%) of each well were laterally connected and contributed to an increase in permeability in the

10.1029/2021WR029888

horizontal direction (Maréchal et al., 2004). However, the highly fractured band did not continue in the vertical direction for a long section and was sandwiched between the less fractured bedrock (i.e., RQD > 76%), indicating the anisotropy of permeability. Therefore, it is unlikely that rapid preferential flow will occur due to vertical fractures (Olofsson, 1994; Salve et al., 2012). As such, fractures are considered to make a small contribution to vertical infiltration in the bedrock. It is highly likely that the hydrological basement surface is defined by the difference in permeability between the C_L and C_M layers, as described in Section 4.4. In addition, there was almost no difference in the density of fractures between the C_L and C_M layers in the F0 watershed (Figure 2); this may be an appropriate general conclusion for the study area.

Since the distribution of fractures was highly heterogeneous, it was difficult to clearly grasp the local connection despite the well density. However, the shape of the BGW table was found to be attributable to the weathering degree of the bedrock, which has a relatively large distribution that can be observed even by indirect exploration methods. For example, the value of electrical resistivity (ER) measured by the indirect exploration method reflects the degree of weathering and the moisture content of the bedrock (e.g., Yamakawa et al., 2012). It is unrealistic to carry out boring surveys at high density in other watersheds; however, it is possible that the BGW catchment area may be estimated by low-cost indirect exploration methods, such as ER methods.

4.6. Conceptual Model of the Bedrock Groundwater Catchment Area

Based on the results obtained using boring wells excavated at high spatial density (61 in bedrock and three in the soil layer) presented above, we developed a conceptual model describing the hydrological processes in a granitic headwater basin controlled by the BGW catchment area. Figure 10 summarizes the process of BGW flow at the study site. According to the matrix K_s of granitic bedrock cores (Table 3), the D and C_L layers are permeable enough to allow a large amount of rainfall to infiltrate if covered with a thick soil layer. However, the C_M layer was nearly impermeable and fractures were considered to make a small contribution to vertical infiltration (Figure 9). As a result, the hydrological basement surface in the bedrock is determined by the shape of the C_L–C_M boundary, which may differ from the surface topography. Vertically infiltrated rainwater reaches the hydrological basement surface and flows as a saturated lateral flow toward the watershed outlet, including cross-watershed flow from adjacent watersheds. For this reason, the BGW catchment area can be determined independently of the surface watershed area (Figure 10).

In this study, the BGW catchment area of the F3 subwatershed expanded to the left and right from the surface watershed border (Figure 5) and was 191% of the watershed area suggested by surface topography (Figure 6). The shapes and areas of BGW catchment areas showed little seasonal change (Figures 5 and 6). The volumetric precipitation input to the BGW catchment area (PV_{BG}) and the volumetric baseflow (QV_B) in 2015 water year was highly correlated (Figure 7d), indicating that the BGW catchment area reflects the actual contributing area in the bedrock layer more accurately than the surface watershed area.

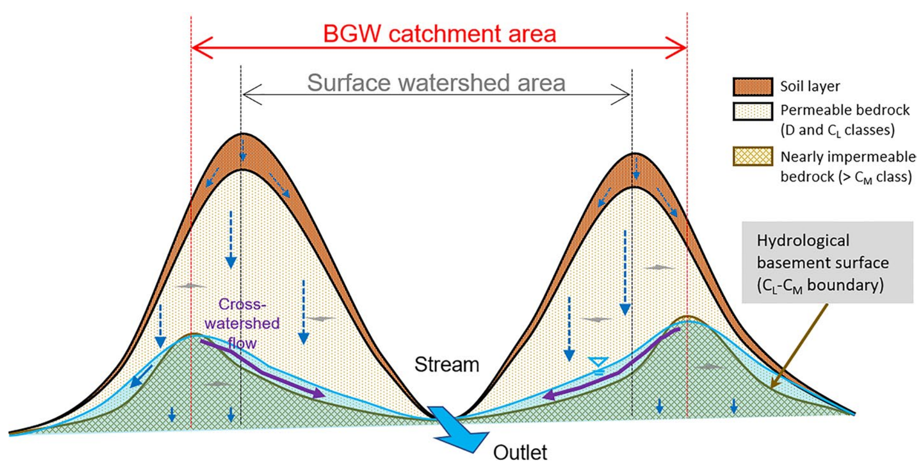

Figure 10. Conceptual model of the bedrock groundwater catchment area.

This concept is considered to fit well in regions having a thick weathered bedrock layer in which matrix K_s is relatively high. In granite, weathering occurs near the surface by dissolving minerals incongruently and extends along fractures (Worthington et al., 2016). However, the process of enhancing bedrock permeability by weathering is critically different depending on the lithology. In future studies, the concept should be updated for regions characterized by fracture-dominant flow (e.g., crystalline rock; Gleeson et al., 2009) or inactive surface/groundwater interaction through less-fractured low permeability bedrock (e.g., conglomerate; Gabrielli et al., 2018).

5. Conclusions

This study demonstrates that (1) the BGW catchment area determined based on the contour map of the water table reflects the actual catchment effect in the bedrock layer more accurately than the surface watershed area. (2) The shape of BGW catchment area is defined by the nearly impermeable surface of the bedrock (i.e., hydrological basement surface). The concept of the BGW catchment area (Figure 10) enables the accurate prediction of streamflow runoff in mountainous headwater basins. It is expected that this concept will be useful for assessing available water resources and predicting flood-related disasters.

At present, the only means to the determine the BGW catchment area is to excavate a high density of boring wells; expanding this to other watersheds is highly impractical. However, it is possible to estimate the BGW catchment area by measuring the baseflow volume due to the high correlation between the two parameters. When combined with indirect exploration methods, such as ER, the distribution of BGW catchment areas may be estimated more accurately. Although this study targets granitic watersheds, it is recommended that research be distributed throughout various watersheds in future as the BGW flow characteristics may differ across watersheds that have unique lithology and weathering process.

Data Availability Statement

Data used in figures and tables are available at https://doi.org/10.14989/264612.

Acknowledgments
The authors thank K. Sugimoto and N. Koinuma of Kyoto Univ. for support in field observations, and S. Matsuishi of Chikousha Co., Ltd., for support in boring the bedrock wells. This work was partly supported by JST, CREST (JPMJCR11R3), and the Fund of Monbukagakusho for Scientific Research (20H00434). The authors also thank two anonymous reviewers, whose insightful and helpful comments greatly improved the manuscript.

References

Asano, Y., Ohte, N., & Uchida, T. (2004). Sources of weathering-derived solutes in two granitic catchments with contrasting forest growth. *Hydrological Processes*, *18*(4), 651–666. https://doi.org/10.1002/hyp.1260

Asano, Y., Uchida, T., & Ohte, N. (2002). Residence times and flow paths of water in steep unchannelled catchments, Tanakami, Japan. *Journal of Hydrology*, *261*(1–4), 173–192. https://doi.org/10.1016/s0022-1694(02)00005-7

Asano, Y., Uchida, T., & Ohte, N. (2003). Hydrologic and geochemical influences on the dissolved silica concentration in natural water in a steep headwater catchment. *Geochimica et Cosmochimica Acta*, *67*(11), 1973–1989. https://doi.org/10.1016/S0016-7037(02)01342-X

Banks, E. W., Simmons, C. T., Love, A. J., Cranswick, R., Werner, A. D., Bestland, E. A., et al. (2009). Fractured bedrock and saprolite hydrogeologic controls on groundwater/surface-water interaction: A conceptual model (Australia). *Hydrogeology Journal*, *17*(8), 1969–1989. https://doi.org/10.1007/s10040-009-0490-7

Brönnimann, C., Stähli, M., Schneider, P., Seward, L., & Springman, S. M. (2013). Bedrock exfiltration as a triggering mechanism for shallow landslides. *Water Resources Research*, *49*, 5155–5167. https://doi.org/10.1002/wrcr.20386

Deere, D. U. (1968). Geological considerations. In K. G. Stagg, & D. C. Ziekiewicz (Eds.), *Rock Mechanics in Engineering Practice* (pp. 1–20). London: Wiley.

Devito, K., Creed, I., Gan, T., Mendoza, C., Petrone, R., Silins, U., & Smerdon, B. (2005). A framework for broad-scale classification of hydrologic response units on the Boreal Plain: Is topography the last thing to consider? *Hydrological Processes*, *19*(8), 1705–1714. https://doi.org/10.1002/hyp.5881

Dickinson, W., & Whiteley, H. (1970). *Watershed areas contributing to runoff* (pp. 12–26). IAHS publication

Dooge, J. C. (1957). The rational method for estimating flood peaks. *Engineering*, *184*(1), 311–313.

Gabrielli, C., Morgenstern, U., Stewart, M. K., & McDonnell, J. J. (2018). Contrasting groundwater and streamflow ages at the Maimai watershed. *Water Resources Research*, *54*(6), 3937–3957. https://doi.org/10.1029/2017wr021825

Garbrecht, J., & Martz, L. W. (1997). The assignment of drainage direction over flat surfaces in raster digital elevation models. *Journal of Hydrology*, *193*(1–4), 204–213. https://doi.org/10.1016/s0022-1694(96)03138-1

Gleeson, T., Novakowski, K., & Kyser, T. K. (2009). Extremely rapid and localized recharge to a fractured rock aquifer. *Journal of Hydrology*, *376*(3–4), 496–509. https://doi.org/10.1016/j.jhydrol.2009.07.056

Hale, V. C., & McDonnell, J. J. (2016). Effect of bedrock permeability on stream base flow mean transit time scaling relations: 1. A multiscale catchment intercomparison. *Water Resources Research*, *52*, 1358–1374. https://doi.org/10.1002/2014wr016124

Haria, A. H., & Shand, P. (2004). Evidence for deep sub-surface flow routing in forested upland Wales: Implications for contaminant transport and stream flow generation. *Hydrology and Earth System Sciences Discussions*, *8*(3), 334–344. https://doi.org/10.5194/hess-8-334-2004

Haria, A. H., & Shand, P. (2006). Near-stream soil water–groundwater coupling in the headwaters of the Afon Hafren, Wales: Implications for surface water quality. *Journal of Hydrology*, *331*(3–4), 567–579. https://doi.org/10.1016/j.jhydrol.2006.06.004

Hewlett, J. D., & Hibbert, A. R. (1967). Factors affecting the response of small watersheds to precipitation in humid areas. In W. E. Sopper, & W. H. Lull (Eds.), *International Symposium on Forest hydrology* (pp. 275–290). New York: Pergamon.

Hinton, M., Schiff, S., & English, M. (1993). Physical properties governing groundwater flow in a glacial till catchment. *Journal of Hydrology*, *142*(1–4), 229–249. https://doi.org/10.1016/0022-1694(93)90012-x

Imamoto, H., Ishigaki, T., & Ohtoshi, K. (1984). Influence factors on refuge of people in the Nagasaki flood disaster in July 1982. *Japan Society for Natural Disaster Science*, *3*(1), 22–33. (in Japanese with English summary).

Inaoka, J., Kosugi, K., Masaoka, N., Itokazu, T., & Nakamura, K. (2020). Effects of geological structures on rainfall-runoff responses in headwater catchments in a sedimentary rock mountain. *Hydrological Processes*, *34*(26), 5567–5579. https://doi.org/10.1002/hyp.13972

Japanese Geotechnical Society. (1979). Engineering properties of weathered granite and granitic soils and their application. *Library of Soil Mechanics and Foundation Engineering*, *16*. 316. (in Japanese (the title is a tentative translation by the authors from the original)).

Jitousono, T., & Haruyama, M. (1985). Quantification of the soil and water conservation function of forest II. Analysis of hydrological data observed in 1983. *Research bulletin of the Kagoshima University forests*, *13*, 159–177. (in Japanese with English summary).

Katsura, S., Kosugi, K., Mizutani, T., & Mizuyama, T. (2009). Hydraulic properties of variously weathered granitic bedrock in headwater catchments. *Vadose Zone Journal*, *8*(3), 557–573. https://doi.org/10.2136/vzj2008.0142

Katsura, S., Kosugi, K., Yamamoto, N., & Mizuyama, T. (2006). Saturated and unsaturated hydraulic conductivities and water retention characteristics of weathered granitic bedrock. *Vadose Zone Journal*, *5*(1), 35–47. https://doi.org/10.2136/vzj2005.0040

Komatsu, Y., & Onda, Y. (1996). Spatial variation in specific discharge of base flow in a small catchments, Oe-yama region, weatern Japan. *Journal of Japan Society of Hydrology and Water Resources*, *9*(6), 489–497. https://doi.org/10.3178/jjshwr.9.489

Kosugi, K., Fujimoto, M., Katsura, S., Kato, H., Sando, Y., & Mizuyama, T. (2011). Localized bedrock aquifer distribution explains discharge from a headwater catchment. *Water Resources Research*, *47*. https://doi.org/10.1029/2010wr009884

Kosugi, K., Katsura, S., Katsuyama, M., & Mizuyama, T. (2006). Water flow processes in weathered granitic bedrock and their effects on runoff generation in a small headwater catchment. *Water Resources Research*, *42*. https://doi.org/10.1029/2005wr004275

Kosugi, K., Katsura, S., Mizuyama, T., Okunaka, S., & Mizutani, T. (2008). Anomalous behavior of soil mantle groundwater demonstrates the major effects of bedrock groundwater on surface hydrological processes. *Water Resources Research*, *44*. https://doi.org/10.1029/2006wr005859

Kosugi, Y., & Katsuyama, M. (2007). Evapotranspiration over a Japanese cypress forest. II. Comparison of the eddy covariance and water budget methods. *Journal of Hydrology*, *334*(3–4), 305–311. https://doi.org/10.1016/j.jhydrol.2006.05.025

Kosugi, Y., Takanashi, S., Tanaka, H., Ohkubo, S., Tani, M., Yano, M., & Katayama, T. (2007). Evapotranspiration over a Japanese cypress forest. I. Eddy covariance fluxes and surface conductance characteristics for 3years. *Journal of Hydrology*, *337*(3–4), 269–283. https://doi.org/10.1016/j.jhydrol.2007.01.039

Maréchal, J. C., Dewandel, B., & Subrahmanyam, K. (2004). Use of hydraulic tests at different scales to characterize fracture network properties in the weathered-fractured layer of a hard rock aquifer. *Water Resources Research*, *40*(11). https://doi.org/10.1029/2004wr003137

Masaoka, N., Kosugi, K., Yamakawa, Y., & Tsutsumi, D. (2016). Processes of bedrock groundwater seepage and their effects on soil water fluxes in a foot slope area. *Journal of Hydrology*, *535*, 160–172. https://doi.org/10.1016/j.jhydrol.2016.01.081

Matsumoto, K., Kosugi, Y., Katsuyama, M., Tani, M., Ohkubo, S., & Takanashi, S. (2011). Estimation of bedrock infiltration on a weathered granitic mountain covered by Japanese cypress forest using water-budget and eddy covariance methods. *International Journal of Erosion Control Engineering*, *4*(1), 10–20. https://doi.org/10.13101/ijece.4.10

Olofsson, B. (1994). Flow of groundwater from soil to crystalline rock. *Hydrogeology Journal*, *2*(3), 71–83. https://doi.org/10.1007/s100400050052

Onda, Y., Komatsu, Y., Tsujimura, M., & Fujihara, J. (2001). The role of subsurface runoff through bedrock on storm flow generation. *Hydrological Processes*, *15*(10), 1693–1706. https://doi.org/10.1002/hyp.234

Payn, R. A., Gooseff, M. N., McGlynn, B. L., Bencala, K. E., & Wondzell, S. M. (2012). Exploring changes in the spatial distribution of stream baseflow generation during a seasonal recession. *Water Resources Research*, *48*. https://doi.org/10.1029/2011wr011552

Pfister, L., Martínez-Carreras, N., Hissler, C., Klaus, J., Carrer, G. E., Stewart, M. K., & McDonnell, J. J. (2017). Bedrock geology controls on catchment storage, mixing, and release: A comparative analysis of 16 nested catchments. *Hydrological Processes*, *31*(10), 1828–1845. https://doi.org/10.1002/hyp.11134

Rinderer, M., McGlynn, B. L., & Van Meerveld, H. J. (2017). Groundwater similarity across a watershed derived from time-warped and flow-corrected time series. *Water Resources Research*, *53*, 3921–3940. https://doi.org/10.1002/2016wr019856

Salve, R., Rempe, D. M., & Dietrich, W. E. (2012). Rain, rock moisture dynamics, and the rapid response of perched groundwater in weathered, fractured argillite underlying a steep hillslope. *Water Resources Research*, *48*. https://doi.org/10.1029/2012wr012583

Sophocleous, M. (2002). Interactions between groundwater and surface water: The state of the science. *Hydrogeology Journal*, *10*(1), 52–67. https://doi.org/10.1007/s10040-001-0170-8

Tromp-van Meerveld, H. J., Peters, N. E., & McDonnell, J. J. (2007). Effect of bedrock permeability on subsurface stormflow and the water balance of a trenched hillslope at the Panola Mountain Research Watershed, Georgia, USA. *Hydrological Processes*, *21*(6), 750–769. https://doi.org/10.1002/hyp.6265

Uchida, T., Asano, Y., Mizuyama, T., & McDonnell, J. J. (2004). Role of upslope soil pore pressure on lateral subsurface storm flow dynamics. *Water Resources Research*, *40*(12). https://doi.org/10.1029/2003wr002139

Uchida, T., Asano, Y., Ohte, N., & Mizuyama, T. (2003a). Analysis of flowpath dynamics in a steep unchannelled hollow in the Tanakami Mountains of Japan. *Hydrological Processes*, *17*(2), 417–430. https://doi.org/10.1002/hyp.1133

Uchida, T., Asano, Y., Ohte, N., & Mizuyama, T. (2003b). Seepage area and rate of bedrock groundwater discharge at a granitic unchanneled hillslope. *Water Resources Research*, *39*(1). https://doi.org/10.1029/2002wr001298

Uchida, T., Asano, Y., Onda, Y., & Miyata, S. (2005). Are headwaters just the sum of hillslopes? *Hydrological Processes*, *19*(16), 3251–3261. https://doi.org/10.1002/hyp.6004

Waddington, J., Roulet, N., & Hill, A. (1993). Runoff mechanisms in a forested groundwater discharge wetland. *Journal of Hydrology*, *147*(1), 37–60. https://doi.org/10.1016/0022-1694(93)90074-j

Welch, L. A., & Allen, D. M. (2014). Hydraulic conductivity characteristics in mountains and implications for conceptualizing bedrock groundwater flow. *Hydrogeology Journal*, *22*(5), 1003–1026. https://doi.org/10.1007/s10040-014-1121-5

Worthington, S. R., Davies, G. J., & Alexander, E. C., Jr (2016). Enhancement of bedrock permeability by weathering. *Earth-Science Reviews*, *160*, 188–202. https://doi.org/10.1016/j.earscirev.2016.07.002

Yamakawa, Y., Kosugi, K., Katsura, S., Masaoka, N., & Mizuyama, T. (2012). Spatial and temporal monitoring of water content in weathered granitic bedrock using electrical resistivity imaging. *Vadose Zone Journal*, *11*(1). https://doi.org/10.2136/vzj2011.0029